28-GHz Channel Measurements and Modeling for Suburban Environments

Yaguang Zhang, Soumya Jyoti, Christopher R. Anderson,
David J. Love, Nicolo Michelusi, Alex Sprintson, and James V. Krogmeier

***Abstract*—This paper presents millimeter wave propagation measurements at 28 GHz for a typical suburban environment using a 400-megachip-per-second custom-designed broadband sliding correlator channel sounder and highly directional 22-dBi (15° half-power beamwidth) horn antennas. With a 23-dBm transmitter installed at a height of 27 m to emulate a microcell deployment, the receiver obtained more than 5000 power delay profiles over distances from 80 m to 1000 m at 50 individual sites and on two pedestrian paths. The resulting basic transmission losses were compared with predictions of the over-rooftop model in recommendation ITU-R P.1411-9. Our analysis reveals that the traditional channel modeling approach may be insufficient to deal with the varying site-specific propagations of millimeter waves in suburban environments. For line-of-sight measurements, the path loss exponents obtained for the close-in (CI) free space reference distance model and the alpha-beta-gamma (ABG) model are 2.00 and 2.81, respectively, which are close to the recommended site-general value of 2.29. The root mean square errors (RMSEs) for these two reference models are 9.93 dB and 9.70 dB, respectively, which are slightly lower than that for the ITU site-general model (10.34 dB). For non-line-of-sight measurements, both reference models, with the resulting path loss exponents of 2.50 for the CI model and 1.12 for the ABG model, outperformed the site-specific ITU model by around 14 dB RMSE.**

I. Introduction

The increasing demand of mobile device users for higher data rates has been the driving factor for the rapid development of mobile telecommunications during the past decade [1]. The number of worldwide mobile subscriptions, which reached a record height of 7.5 billion in 2016, has continued to increase, and the total mobile data traffic is expected to rise at a compound annual growth rate of 42% between the end of 2016 and 2022 [2]. This increasing usage of wireless technology is prompting mobile service providers to take advantage of higher frequency bands in the foreseeable future, starting with millimeter waves (mm-waves), to overcome the expected global bandwidth shortage [3].

With recent advances in radio frequency (RF) technology [4]–[6], hardware operating at mm-wave frequencies is becoming commercially available [7]–[9]. This has made mm-wave frequencies the most promising higher frequency bands for a larger usable radio spectrum. To fully understand the propagation characteristics of mm-wave signals, the amount of research on mm-wave channel measurement and modeling has increased dramatically in the past five years [1], [10]–[12]. However, the majority of current research on mm-wave communications has focused on urban areas with high population densities, with very few measurement campaigns in suburban and rural environments, which are also important for future mobile networking technologies. Moreover, statistical models for point-to-point links have received significant attention, but the channel information provided by these approaches is insufficient for next-generation wireless networks such as 5G. These networks must address mobility requirements because frequent and location-specific blockages are expected at mm-waves, which require a much richer set of channel state information beyond LoS path loss (such as multipath scattering).

In this paper, we explore this gap in the research by focusing on suburban environments and constructing physically-motivated and practical models that can be used for mm-wave networks in these environments. An intensive measurement campaign has been carried out at the United States Naval Academy (USNA) in Annapolis, Maryland. Measurements were taken around the campus at 28 GHz to characterize the propagation in a suburban-type environment. The resulting path losses are compared with several standard 5G channel models. Our results indicate that a holistic, network-wide approach beyond traditional point-to-point links may be needed to deal with the high dependence of mm-waves on site-specific environment geometry.

The paper is organized as follows. In Section II, we present our propagation measurements in suburban environments. The results, together with our analyses, are described in Section III. Finally, in Section IV, we conclude the paper.

II. Mm-Wave Propagation Measurements for Suburban Environments

An outdoor propagation measurement campaign was conducted on the USNA campus to emulate a typical 5G deployment in a suburban environment. Compared with urban environments, the USNA campus has shorter buildings with more flexible shapes and locations, wider streets, and lighter traffic. During the campaign, the transmitter (TX) was temporarily installed on the Mahan Hall clock tower. The receiver

Y. Zhang, D. J. Love, N. Michelusi, and J. V. Krogmeier are with the School of Electrical and Computer Engineering, Purdue University, 465 Northwestern Avenue, West Lafayette, IN 47907, USA. (Email: {ygzhang, djlove, michelus, jvk}@purdue.edu)

C. R. Anderson is with the Department of Electrical and Computer Engineering, United States Naval Academy, 105 Maryland Ave, Annapolis, MD 21402, USA. (Email: canderso@usna.edu)

S. Jyoti and A. Sprintson are with the Department of Electrical and Computer Engineering, Texas A&M University, College Station, TX 77843, USA. (Email: {soumyajyoti.jh, spalex}@tamu.edu)

Sponsorship for this work was provided by NSF under grant CNS-1642982.

978-1-5386-3180-5/18/$31.00 ©2018 IEEE

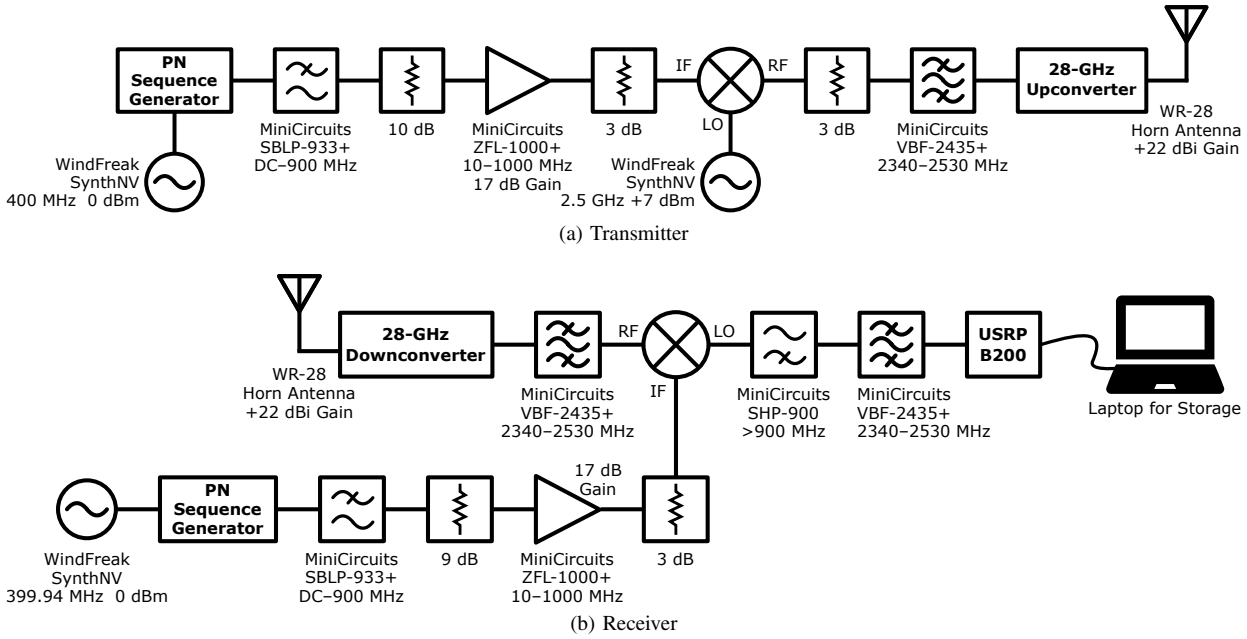

Fig. 1. Block diagrams for the 28-GHz broadband sliding correlator channel sounder. Model numbers are labeled for some commercially available parts.

(RX) was moved around the campus to obtain path loss measurements for individual sites and continuous paths. More details for the measurement setup can be found in [13].

A. Measurement Equipment

A custom-designed broadband sliding correlator channel sounder [14] was used to record propagation data. Fig. 1 presents block diagrams for the channel sounder. At both the TX and the RX sides, horn antennas with a nominal +22 dBi gain and 15° half-power beamwidth (HPBW) were employed, and pseudo-random noise (PN) generators produced the same PN sequences with a chip sequence length of 2047 [1].

At the TX, the PN probing signal was generated with a chip rate of 400 megachips per second (Mcps). To make the implementation cost-effective, the signal was first modulated to a 2.5-GHz intermediate frequency (IF) and then converted to RF of 28 GHz by mixing it with a 25.5-GHz local oscillator (LO) at the upconverter. At the RX, the received signal was first downconverted from 28 GHz to 2.5 GHz and then cross-correlated with the identical PN sequence generated with a slightly slower clock rate of 399.94 MHz, similar to the setup in [1]. A Universal Software Radio Peripheral (USRP) B200 was utilized to record the resulting in-phase (I) and quadrature (Q) signal components. It also regularly sampled the RX's location with the help of an on-board GPS disciplined oscillator (TCXO version).

Table I summarizes the key parameters for the channel sounder. Note that the estimation for the maximum measurable path loss is based on the following. (1) The RX low-noise amplifier has a noise figure of 2.4 dB, so we assume a worst-case RX noise figure of 6 dB. (2) The RX detection bandwidth is 60 kHz. (3) The minimum signal-to-noise ratio (SNR) for a detectable signal is empirically estimated as 5 dB.

TABLE I
BROADBAND SLIDING CORRELATOR CHANNEL SOUNDER SPECIFICATIONS

Carrier Frequency	28 GHz
Chip Sequence Length	2047
RF Bandwidth (First Null)	800 MHz
TX Chip Rate	400 Mcps
Temporal Resolution	2.5 ns
RX Chip Rate	399.94 Mcps
TX Power	23 dBm
TX/RX Antenna Gain	22 dBi
Measured TX/RX Azimuth HPBW	10.1°
Measured TX/RX Elevation HPBW	11.5°
Maximum Measurable Path Loss	182 dB

B. Measurement Setup and Procedure

Three types of measurements have been performed for large-scale path loss, emulated single-input and multiple-output (SIMO), and continuous tracks. The TX was installed at a height of 90 feet (27.4 m) to emulate a microcell deployment. The RX was moved around campus by an electric car or a two-layer platform trolley to obtain the measurements, which is illustrated by the photographs in Fig. 2.

We used compasses and digital levels to achieve beam alignment prior to measurements at each RX location. Aside from the USRP output files and GPS samples, the azimuths and elevations of both the TX and RX antennas were recorded manually. This allowed us to reconstruct the geometry relationship of the antennas and extract precise antenna gains during post-processing for path loss computation and analysis. The USRP gain was manually adjusted to maximize the RX SNR.

(a) RX on an Electric Car

(b) RX on a Trolley

(c) Before a Continuous Signal Recording for a Pedestrian Path

Fig. 2. Photos of the measurement setup. The TX was installed on a clock tower at a height of 90 feet (27.4 m) to emulate a microcell deployment. Either an electric car or a two-layer trolley was used to transport the RX. For both cases, the platform for the RX could be rotated horizontally and tilted with composite wood shims to align the beam.

1) Large-Scale Path Loss Measurements: Forty measurement locations were chosen to investigate the large-scale path loss at various distances from the TX (between 100 m and 1000 m). For each site, the RX antenna was moved along X and Z axes by a custom-built positioning system (see Fig. 2b and Fig. 2c) to form a "+" pattern within a $20\lambda \times 20\lambda$ area, where $\lambda = 10.7$ mm was the wave length corresponding to 28 GHz. For every λ interval on the "+" pattern, one 3-second signal recording and one GPS sample were obtained, which ended up with 40 separate measurements in total for one site.

2) Emulated SIMO Measurements: Measurements that were used to emulate SIMO signals were similar to those for the large-scale path loss, but with a higher space sample density and a larger sample area for each site. The RX antenna was moved along the "+" pattern with the interval between adjacent measurements reduced to 0.25λ. The pattern covered an enlarged $40\lambda \times 40\lambda$ area, with 320 separate measurements in total for each site. Ten locations were chosen, where the distances between the TX and the RX varied from 50 m to 500 m. The data collected were or will be used to analyze small-scale propagation characteristics. However, in this paper, we focus only on the large-scale path loss.

3) Measurements for Continuous Tracks: To investigate the shadowing effect on a moving user, two approximately 200-m-long straight tracks were chosen for continuous signal recordings. The TX antenna was pointed at the center of the track for each recording. The RX antenna was fixed on the positioning system and moved at walking speed along each track to record the signal, and the GPS location of the RX was sampled once per second. The RX antenna elevation was kept at 0°, and the platform was adjusted as necessary to maintain the azimuth with respect to the fixed earth reference during the recording process (see Fig. 2c) for the beam alignment.

III. Measurement Results and Analysis

After signal recordings and GPS samples were collected during the measurement campaign, post-processing was carried out for computing the basic transmission loss. Received signal power calculation, RX calibration, antenna pattern generation, and antenna gain extraction were considered in determining antenna-independent path losses. The detailed procedures for them can be found in [13]. In Fig. 3, 49 of the 50 static sites are shown on a Google map of the USNA campus. One large-scale site was ignored in our analysis because the data collected there were influenced by rain.

A. Line-of-Sight (LoS) Sites

For LOS sites (24 in total), we compared the measurement results with the International Telecommunication Union (ITU) site-general model for propagation over rooftops [15]:

$$PL(d,f) = 10 \cdot \alpha \cdot \log_{10}(d) + \beta + 10 \cdot \gamma \cdot \log_{10}(f) + N(0,\sigma), \quad (1)$$

where d is the 3D direct distance between the TX and the RX in meters and f is the operating frequency in GHz. In our case, $f = 28$ GHz. The parameter values $\alpha = 2.29$, $\beta = 28.6$, $\gamma = 1.96$, and $\sigma = 3.48$, were chosen for the LoS propagation in a suburban environment [15], which are recommended by ITU for distances from 55 m to 1200 m at 2.2–73 GHz frequency.

For a better comparison, we also considered two other models as references. The first is the close-in (CI) free space reference distance path loss model:

$$PL(d) = PL_{FS}(d_0) + 10 \cdot n \cdot \log_{10}\left(\frac{d}{d_0}\right), \quad (2)$$

$$PL_{FS}(d_0) = 20 \cdot \log_{10}\left(\frac{4\pi d_0}{\lambda}\right), \quad (3)$$

where n is the path loss exponent, $PL_{FS}(d_0)$ is the free-space propagation loss at a distance of $d_0 = 1$ m with isotropic antennas, and λ is the carrier wavelength. The second is the alpha-beta-gamma (ABG) model on which the ITU site-general model is based:

$$PL(d) = 10 \cdot \alpha \cdot \log_{10}(d) + \beta + 10 \cdot \gamma \cdot \log_{10}(f). \quad (4)$$

Note that α here acts as the path loss exponent.

We have fit these two reference models to our LoS measurement results. To deal with GPS sample errors, the median values of latitude, longitude, and altitude measurements for each site were used as that site's geographic location to compute the site distance to the TX. And for the ABG model, we set $\gamma = 1.96$ as recommended by ITU, given that we had only one carrier frequency at 28 GHz.

All three models, together with the measurement results, are presented in Fig. 4a. The ITU model provides path loss

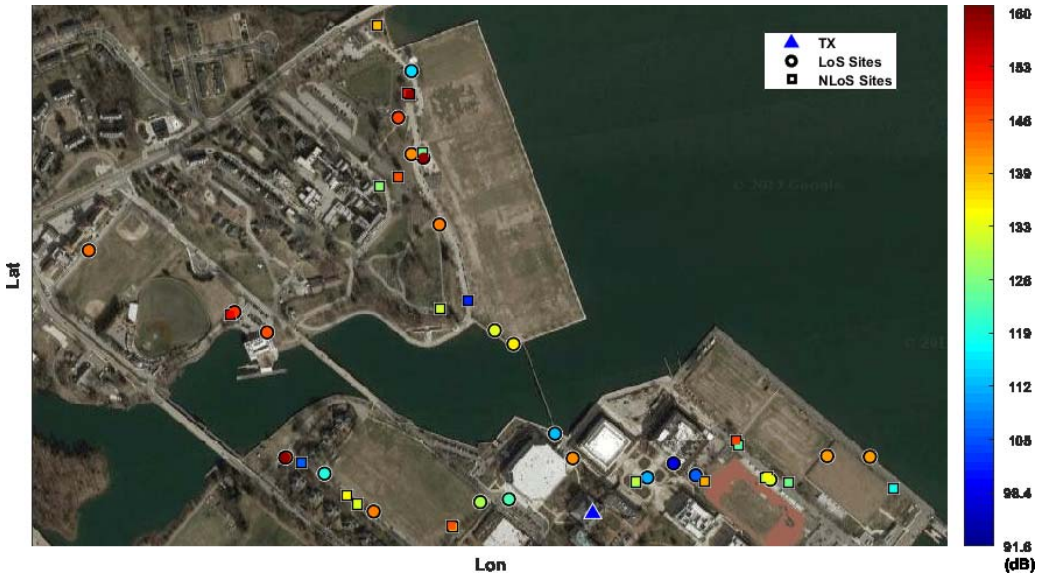

Fig. 3. Overview for the basic transmission losses of the large-scale and SIMO measurements. The geographic locations for the measurement sites are shown on a Google map of the USNA campus, with their corresponding worst-case basic transmission losses illustrated by color labels.

predictions in the form of Gaussian variables, and their 3-sigma range covers the measured path losses reasonably well, even though if we extrapolate the ITU model to $d = d_0 = 1$ m, its mean path loss would be smaller than the corresponding free-space propagation loss (FSPL). This issue affects the ABG type of models in general. In our case, the ABG model has the lowest root mean square error (RMSE) at 9.70 dB, but its predicted path loss quickly descends below FSPL as the distance decreases. Hence, the ABG model does not generalize well outside the distance range for its measurement data.

The resulting path loss exponents for the CI and ABG reference models are 2.00 and 2.81, respectively. For the LoS dataset, these two models perform 0.41 dB and 0.64 dB better than the ITU model, respectively, in RMSE. Basically, within the distance range of the LoS measurement dataset, these three models are equivalent, and the ITU model performs well.

The four sites with lower path losses than the ITU 3-sigma range were further investigated through their PDPs. As very strong multipath components were observed for all of these sites, it is still possible for even narrow mm-waves to have multipath components that dramatically enhance the signal. For the closer two sites, this was expected because they were surrounded by buildings. However, the two sites at farther distances were in open areas, and the most reasonable origins of the multipath were reflections from buildings close to the TX, as many of these buildings have sloped ceilings.

B. Non-Line-of-Sight (NLoS) Sites

For the 25 NLoS sites, the site-specific model for propagation over rooftops defined in ITU-R P.1411-9, Section 4.2.2.2 [15] was utilized to predict the path loss for each site. Similar to the LoS case, the CI and ABG models were compared with the ITU model as references. This time, γ was set to 2.30 for the ABG model, as recommend by ITU for NLoS above-rooftop propagation from 260 m to 1200 m at 2.2–66.5 GHz in an urban high-rise environment, which was the most suitable for our purposes.

TABLE II
KEY PARAMETERS FOR CHANNEL MODELS

Model	LoS					NLoS				
	n	α	β	γ	RMSE (dB)	n	α	β	γ	RMSE (dB)
ITU	N/A	2.29	28.6	1.96	10.34	N/A	N/A	N/A	N/A	25.33
CI	2.00	N/A	N/A	N/A	9.93	2.50	N/A	N/A	N/A	11.73
ABG	N/A	2.81	11.66	1.96	9.70	N/A	1.12	63.61	2.30	11.05

Fig. 4b shows the ITU predictions together with the reference models and NLoS measurement results. For the NLoS data, the ITU model shows a trend of following the measured path loss, but it has over-estimated predictions for most of the sites. Only five of the NLoS sites had measured path losses that were clearly larger than the corresponding ITU predictions. Furthermore, the ABG model does not agree well with the CI model, with resulting path loss exponents of 1.12 and 2.50, respectively. This may be caused by an over-fitting of the ABG model to our NLoS path losses. However, both of these reference models outperformed the ITU predictions by around 14 dB in RMSE. Table II summarizes the key parameters for the obtained channel models.

Several factors may have reduced the performance of the ITU site-specific model. First, buildings on the USNA campus are not geometrically arranged exactly like those defined in the ITU suburban area propagation model. The over-rooftop propagations often span multiple building rows, which alters the blockage and reflection conditions. Also, for many of our sites, the ITU over-rooftop model with a limited number of buildings would be a better fit, which may ameliorate the path

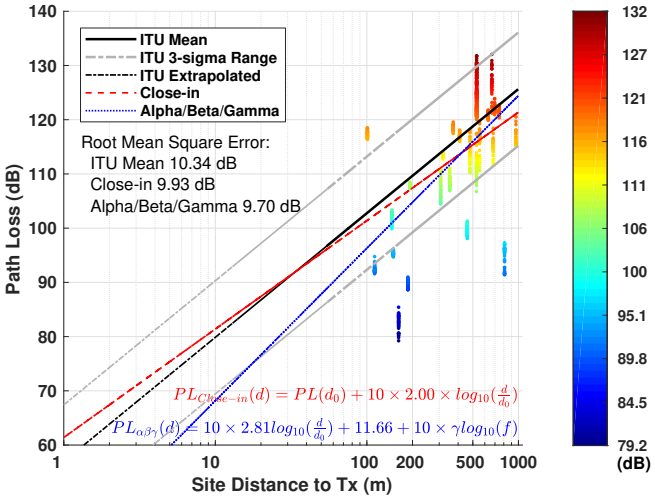

(a) For the LoS Measurements

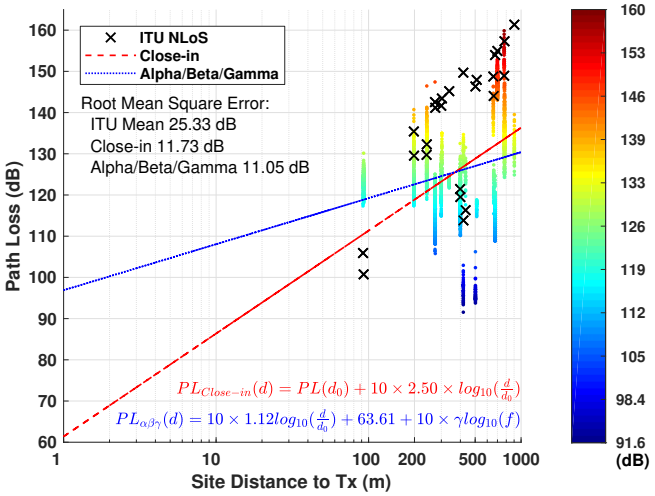

(b) For the NLoS Measurements

Fig. 4. Model comparison for LoS and NLoS measurements. (a) In the LoS case, the ITU predictions agree reasonably well with our measurement results and the reference models. (b) For NLoS sites, the ITU predictions show a trend of following the measurement results but overestimate the path loss for most of these sites.

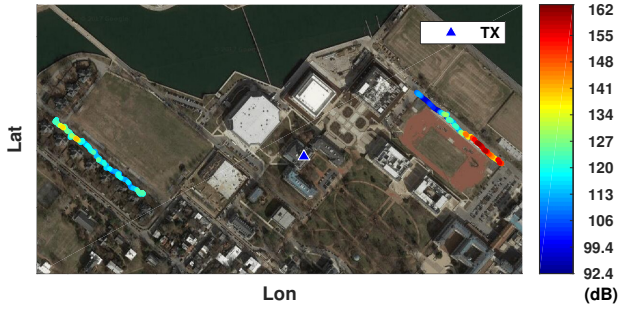

(a) Basic Transmission Losses for Continuous Tracks Shown on a Google Map of the USNA Campus

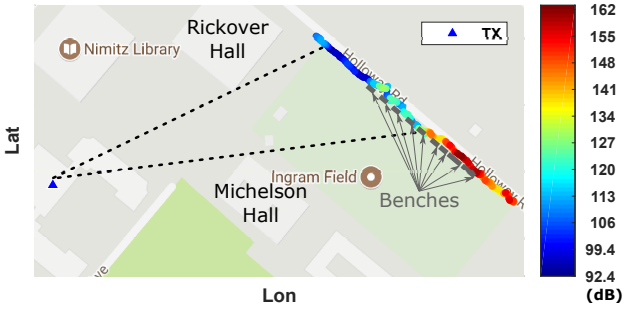

(b) Track on Holloway Road

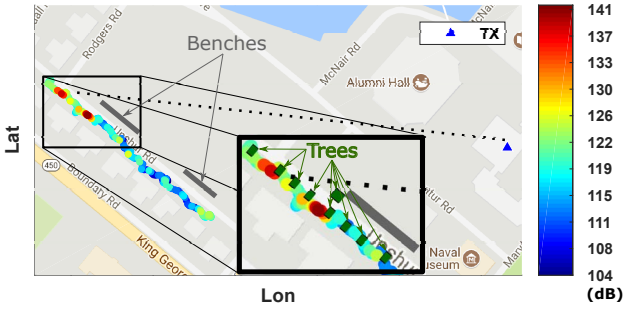

(c) Track on Upshur Road

Fig. 5. Basic transmission losses for continuous tracks. The path losses on Holloway road illustrate the shadowing effect of buildings and benches, while those on Upshur road illustrate the shadowing effect of trees. In (c), the starting part of the track is zoomed in, and trees are indicated by green rectangles.

loss overestimation for propagations beyond the building area.

Second, the parameter ranges defined in the ITU model do not always agree with those for our NLoS sites. For example, the street width for most of our sites was over the defined limit. For these cases, we used the upper bound for the model, 25 m, in the calculation, so the model may have underestimated the path losses for sites relatively close to the TX by considering reflections from buildings that do not exist. For sites that were further away, more buildings are positioned between the TX and the RX, which may have caused an overestimation.

Third, at around 10 of the NLoS sites, the LoS propagation was directly blocked by vegetation, not buildings [16]. A few other sites have foliage near their LoS paths. ITU-R P.1411-9 does not consider the propagation effects caused by vegetation due to the complexity.

C. Continuous Tracks

Two continuous signal recordings were conducted to investigate the shadowing effect on a simulated moving user at walking speed. The basic transmission losses were calculated for each second of the signal recordings (see Fig. 5).

For the track on Holloway road (Fig. 5b), the most significant blockage was from Michelson Hall, which caused approximately 30 dB of additional path loss to half of the track. Rickover Hall partially blocked the track by around 20 dB. The dotted lines in Fig. 5b show where these blockages started on the track. There were also metal stadium benches on the northeast side of Ingram Field adjacent to the measurement route, which caused around 20 dB of additional path loss. This is more clear on the part of the track with no building blockages, where a path loss peak shows up behind each one of the benches.

For the track on Upshur road (Fig. 5c), the two benches next to the measurement route were farther away from the track and did not block the signal significantly. For this set of data, the effect of foliage shadowing is of interest. Trees were planted on the TX side adjacent to the pathway, and a few path loss peaks shown on Fig. 5c correspond well with the locations of these trees.

D. Discussion

We have focused on the large-scale path loss, comparing our measurements with predictions obtained by following ITU-R P.1411-9 [15] on propagation over rooftops. Our data show that a richer set of channel state information, including multipath scattering and location-specific building geometries, are necessary to produce more reliable coverage predictions. In the LoS situation, the measurements agree reasonably well with the ITU predictions, while for the NLoS situation, most of the predictions appear to have higher path losses than the corresponding measurement results. Limiting the building number, extending the model with sloped ceilings, and considering over-rooftop propagations spanning multiple building rows may help improve the ITU site-specific model for suburban environments.

Based on the model comparison, the CI and ABG models do a good job of predicting large-scale path loss in both LoS and NLoS cases. Furthermore, the ABG model, in general, is able to provide a better fit for a given set of data. However, it may give non-physical results beyond the distance range over which the data are collected. Because of this, care should be taken for results out of the ABG model's defined range.

The continuous recordings back up channel modeling attempts that consider environmental information, for example, through the radio environment map [17] and ray tracing [18]. Moreover, the results indicate it is possible to increase large-scale path loss prediction accuracy for statistical models with simple but site-specific environment geometry, which would balance the computation complexity and the model performance. In the future, we will investigate the possibility of improving the ITU models with cite-specific geometric features, which are either completely ignored or only partially captured within the current ITU modeling processes.

IV. Conclusion

In this paper, we discussed the implementation of a custom-designed broadband channel sounder and explained how we used it for a measurement campaign that focused on the propagation of mm-waves in suburban environments at 28 GHz. The resulting basic transmission losses for LoS and NLoS sites were separately compared with the corresponding propagation predictions based on the ITU-R P.1411-9 recommendation. The site-general LoS model for propagation over rooftops in suburban environments agreed with our measurements reasonably well, but the corresponding site-specific NLoS model overestimated the path loss for most of the NLoS sites. Two continuous measurement tracks were also constructed. The results illustrated that a knowledge of geometric features may increase the prediction performance for large-scale path losses, which backs up the radio environment map approach for channel modeling in future communication networks.

Acknowledgment

We would like to thank the faculty members from the Department of Electrical and Computer Engineering at USNA for their kind assistance during the measurement campaign.

References

[1] T. S. Rappaport, *et al.*, "Millimeter wave mobile communications for 5g cellular: It will work!" *IEEE access*, vol. 1, pp. 335–349, 2013.

[2] "Ericsson mobility report june 2017," Ericsson, SE-164 80 Stockholm, Sweden, Tech. Rep., June 2017. [Online]. Available: https://www.ericsson.com/assets/local/mobility-report/documents/2017/ericsson-mobility-report-june-2017.pdf

[3] T. S. Rappaport, R. W. Heath Jr, R. C. Daniels, and J. N. Murdock, *Millimeter Wave Wireless Communications*. Pearson Education, 2014.

[4] K. Okada, *et al.*, "Full four-channel 6.3-gb/s 60-ghz cmos transceiver with low-power analog and digital baseband circuitry," *IEEE Journal of Solid-State Circuits*, vol. 48, no. 1, pp. 46–65, 2013.

[5] N. Saito, *et al.*, "A fully integrated 60-ghz cmos transceiver chipset based on wigig/ieee 802.11 ad with built-in self calibration for mobile usage," *IEEE Journal of Solid-State Circuits*, vol. 48, no. 12, pp. 3146–3159, 2013.

[6] D. Fritsche, G. Tretter, C. Carta, and F. Ellinger, "Millimeter-wave low-noise amplifier design in 28-nm low-power digital cmos," *IEEE Transactions on Microwave Theory and Techniques*, vol. 63, no. 6, pp. 1910–1922, 2015.

[7] Z. Pi and F. Khan, "An introduction to millimeter-wave mobile broadband systems," *IEEE Communications Magazine*, vol. 49, no. 6, 2011.

[8] S. Rangan, T. S. Rappaport, and E. Erkip, "Millimeter-wave cellular wireless networks: Potentials and challenges," *Proceedings of the IEEE*, vol. 102, no. 3, pp. 366–385, 2014.

[9] W. Roh, *et al.*, "Millimeter-wave beamforming as an enabling technology for 5g cellular communications: Theoretical feasibility and prototype results," *IEEE Communications Magazine*, vol. 52, no. 2, pp. 106–113, 2014.

[10] G. R. MacCartney and T. S. Rappaport, "73 ghz millimeter wave propagation measurements for outdoor urban mobile and backhaul communications in new york city," in *IEEE International Conference on Communications (ICC), 2014*. IEEE, 2014, pp. 4862–4867.

[11] A. I. Sulyman, A. T. Nassar, M. K. Samimi, G. R. Maccartney, T. S. Rappaport, and A. Alsanie, "Radio propagation path loss models for 5g cellular networks in the 28 ghz and 38 ghz millimeter-wave bands," *IEEE Communications Magazine*, vol. 52, no. 9, pp. 78–86, 2014.

[12] S. Deng, M. K. Samimi, and T. S. Rappaport, "28 ghz and 73 ghz millimeter-wave indoor propagation measurements and path loss models," in *IEEE International Conference on Communication Workshop (ICCW), 2015*. IEEE, 2015, pp. 1244–1250.

[13] Y. Zhang, *et al.*, "28-ghz channel measurements and modeling for suburban environments," Department of Electrical and Computer Engineering, Purdue University, West Lafayette, Indiana, Tech. Rep. TR-ECE-17-07, November 2017.

[14] T. S. Rappaport, *et al.*, *Wireless Communications: Principles and Practice*. New Jersey: Prentice Hall PTR, 1996, vol. 2.

[15] ITU, "Propagation data and prediction methods for the planning of short-range outdoor radiocommunication systems and radio local area networks in the frequency range 300mhz and 100ghz," Tech. Rep., June 2017. [Online]. Available: https://www.itu.int/rec/R-REC-P.1411-9-201706-I/en

[16] Y. Zhang, *et al.*, "Improving millimeter-wave channel models for suburban environments with site-specific geometric features," in *International Applied Computational Electromagnetics Society Symposium (ACES)*, 2018, to be published.

[17] H. B. Yilmaz, T. Tugcu, F. Alagoz, and S. Bayhan, "Radio environment map as enabler for practical cognitive radio networks," *IEEE Communications Magazine*, vol. 51, no. 12, pp. 162–169, 2013.

[18] T. A. Thomas, H. C. Nguyen, G. R. MacCartney, and T. S. Rappaport, "3d mmwave channel model proposal," in *IEEE 80th Vehicular Technology Conference (VTC Fall), 2014*. IEEE, 2014, pp. 1–6.